Research in Astronomy and Astrophysics, 23:105003 (6pp), 2023 October https://doi.org/10.1088/1674-4527/ace51d

A Pulsar Wind Nebula Origin of the Ultra-high-energy Source 1LHAASO J1929+1846

Qi Xia, Lian-Cheng Zhou, and Jun Fang
Department of Astronomy, Yunnan University, Kunming 650091, China; fangjun@ynu.edu.cn
Received 2023 April 21; revised 2023 June 18; accepted 2023 June 25; published 2023 September 19

Abstract

1LHAASO J1929+1846 is one of the ultra-high-energy (UHE, $E > 0.1$ PeV) sources in the first catalog of γ-ray sources detected by the Large High Altitude Air Shower Observatory. It has been detected fluxes at 3 TeV for $2.48 \pm 0.11 \times 10^{-13}$ TeV^{-1} cm^{-2} s^{-1} with the Water Cherenkov Detector Array and at 50 TeV for $0.64 \pm 0.06 \times 10^{-16}$ TeV^{-1} cm^{-2} s^{-1} with the Kilometer Squared Array, but the origin of its UHE emission remains unknown. The pulsar wind nebula (PWN) G54.1+0.3, which is powered by the pulsar PSR 1930+1852 with a period of 136 ms and it is detected within a $0.^{\circ}29$ region around the centroid of 1LHAASO J1929+1846. We explore whether G54.1+0.3 is capable of producing the UHE radiation of 1LHAASO J1929+1846. First, the data with Fermi Large Area Telescope for the PWN is analyzed to obtain the GeV fluxes. Second, the multiband non-thermal fluxes for the nebula are investigated based on a one-zone time-dependent model. In the model, we assume the spin-down energy of the pulsar is persistently injected into particles (electrons and positrons) and magnetic field in the PWN, and these high-energy particles produce multiband non-thermal radiation from radio to γ-rays via synchrotron radiation and inverse Compton scattering. We reproduce the spectral energy distribution of PWN G54.1+0.3 with reasonable parameters. The result indicates that the UHE γ-ray source 1LHAASO J1929+1846 possibly originates from PWN G54.1+0.3.

Key words: radiation mechanisms: non-thermal – ISM: supernova remnants – gamma-rays: stars

1. Introduction

With the developments of γ-ray detectors, not only multiple very-high-energy (VHE, $E > 0.1$ TeV) γ-ray sources, but also more and more ultra-high-energy (UHE, $E > 0.1$ PeV) γ-ray sources are discovered (H.E.S.S. Collaboration et al. 2018; Abeysekara et al. 2020; Cao et al. 2021; Joshi et al. 2023). That indicates there are celestial objects in galaxy, PeVatrons, which can accelerate Cosmic rays (CRs) to PeV energies and generate UHE γ-rays. The propagation of γ-rays is not influenced by the magnetic fields in interstellar space. Researching the γ-rays emission from MeV to TeV, even to PeV energies, is one of the important means to investigate indirectly the generation, acceleration and propagation mechanism of CRs. As a class of Galactic TeV γ-ray sources, there are relativistic shocks in nebulae and it can accelerate energy of particles to hundreds TeV even PeV energies, thus producing radiation from the radio band to the TeV band. The previous studies indicate that PWNe have the ability to produce the γ-rays with energy above 100 TeV (Fang et al. 2020; Zhang et al. 2020; Liu & Wang 2021; Liang et al. 2022; Yu et al. 2022; Joshi et al. 2023; Wu et al. 2023). Thus, deeply theoretical studies for UHE γ-ray sources based on comprehensive multiband observations are necessary for understanding production, transmission and radiation mechanisms of CRs.

The Large High Altitude Air Shower Observatory (LHAASO) is a complex of extensive air shower (EAS) detector arrays and it consists of three interconnected detectors: WCDA, Kilometer Squared Array (KM2A) and Wide Field-of-view Cherenkov Telescope Array (WFCTA), which is located at 4410 m above sea level in Sichuan Province, China (Cao 2010). Cao et al. (2023) made a noteworthy announcement, unveiling the first catalog of VHE and UHE sources detected by the LHAASO, which was achieved by analyzing 508 days of data collected by the WCDA and 933 days of data recorded by the KM2A. 1LHAASO J1929+1846 is one of the UHE sources in the first catalog of γ-ray sources, which had been detected fluxes at 3 TeV for $2.48 \pm 0.11 \times 10^{-13}$ TeV^{-1} cm^{-2} s^{-1} with WCDA and at 50 TeV for $0.64 \pm 0.06 \times 10^{-16}$ TeV^{-1} cm^{-2} s^{-1} with KM2A (Cao et al. 2023). It is worth noting that the nearest TeV counterpart found within the search radius is supernova remnant (SNR) G54.1+0.3, which is a pulsar wind nebula (PWN) located within $0.^{\circ}29$ of the center of 1LHAASO J1929+1846 (Cao et al. 2023). Motivated by their research, based on a one-zero time-dependent model for the multiband non-thermal emission of PWN and combined with observed data from the radio to the TeV band, we have investigated whether PWN G54.1+0.3 is capable of producing the UHE radiation of 1LHAASO J1929+1846.

The γ-ray source PWN G54.1+0.3 was first observed at 4.75 GHz (Reich et al. 1985) and Velusamy & Becker (1988) identified it as a Crab-like SNR, also known as PWN, with the observation results of VLA, OSRT and IRAS. Lu et al. (2002) revealed its X-ray non-thermal spectrum, the ring and the bipolar jet morphology, which confirmed G54.1+0.3 to be a PWN. Moreover, Lu et al. (2001) obtained the spectrum and an image of G54.1+0.3 with the ROSAT PSPC, ASCA SIS and GIS observations. The image clearly shows an X-ray jet, which is consistent with the radio extension to the northeast in both direction and position, therefore they propose that the jet is connected with the pulsar that is assumed to exist in the remnant. One year later, the pulsar PSR 1930+1852 powering PWN G54.1+0.3, was discovered by Camilo et al. (2002) in radio with a period of 136 ms. After that, Lu et al. (2007) confirmed it as a typical Crab-like pulsar based on the observation data of the Rossi X-Ray Timing Explorer (RXTE) and Chandra X-ray observatories. At the TeV-band, Abeysekara et al. (2018) confirmed that PWN G54.1+0.3 is the counterpart of the γ-ray source, VER J1930+188 and 2HWC J1930+188.

In this paper, based on a one-zone time-dependent model for the multiband non-thermal emission from PWNe with reasonable parameters, using updated TeV fluxes observed with the Fermi Large Area Telescope (Fermi-LAT), the Very Energetic Radiation Imaging Telescope Array System (VERITAS), the latest High Altitude Water Cherenkov (HAWC) and the LHAASO, we modeled the spectral evolution of G54.1+0.3 and investigated whether PWN G54.1+0.3 is able to produce the UHE radiation of 1LHAASO J1929+1846. In Section 2, the model is briefly described. In Section 3, we show the results from the model and compare the results with the observations. In Section 4, the discussions and summary are given.

2. The Model for the Multiband Non-thermal Emission from PWNe

In this paper, the evolution of the spectrum of the high-energy electrons/positrons in a PWN on time, i.e., $N(\gamma, t)$, is solved according to the equation (Martín et al. 2012),

$$\frac{\partial N(\gamma, t)}{\partial t} = -\frac{\partial}{\partial \gamma}[\dot{\gamma}(\gamma, t)N(\gamma, t)] - \frac{N(\gamma, t)}{\tau(\gamma, t)} + Q(\gamma, t), \tag{1}$$

where $\dot{\gamma}(\gamma, t)$ represents the energy loss rate due to synchrotron radiation, inverse Compton, and adiabatic expansion, $\tau(\gamma, t)$ is the time of the particles escaping from the nebula, and $Q(\gamma, t)$ is the injection rate of the particles. A broken power law spectrum is usually adopted for the injected particles, i.e.,

$$Q(\gamma, t) = Q_0(t)\begin{cases}\left(\frac{\gamma}{\gamma_b}\right)^{-\alpha_1} & \gamma \leqslant \gamma_b \\ \left(\frac{\gamma}{\gamma_b}\right)^{-\alpha_2} & \gamma_b < \gamma \leqslant \gamma_{max}\end{cases}, \tag{2}$$

where α_1, α_2 are the spectral indices. γ_{max} is limited according to $R_L = \epsilon R_s$, where R_L and R_s are the Larmor radius and the radius of the termination.

The spin-down energy of the pulsar powering the nebula is transferred into particles and magnetic field. For a given magnetic energy fraction η, the magnetic field strength in the PWN equals (Tanaka & Takahara 2010; Martín et al. 2012)

$$B(t) = \sqrt{\frac{3(n-1)\eta\tau_0 L_0}{R_{PWN}^3(t)}\left[1 - \left(1 + \frac{t}{\tau_0}\right)^{-\frac{2}{n-1}}\right]}, \tag{3}$$

where n is the braking index, L_0 is the initial luminosity and τ_0 is spin-down timescale of the pulsar. The radius of the nebula, R_{PWN}, which is given by van der Swaluw et al. (2001)

$$R_{PWN}(t) = C\left(\frac{L_0 t}{E_0}\right)^{1/5}\left(\frac{10E_0}{3M_{ej}}\right)^{1/2} t, \tag{4}$$

where C is a constant and M_{ej} is the mass of ejected when supernova (SN) explosion. The other details of the model for the multiband non-thermal emission from a PWN can be seen in (Martín et al. 2012).

3. Results

The PWN G54.1+0.3, which was first observed by Reich et al. (1985) at 4.75 GHz, also detected with VERITAS, HAWC and H.E.S.S., thus was known as VER J1930+188, 2HWC J1930+188, and HESS J1930+188. The PWN is powered by the pulsar PSR 1930+1852 with a period of $P = 136$ ms, $\dot{P} = 7.5 \times 10^{-13}$ s s^{-1} and an assumed breaking index $n = 3$. Based on these parameters, we can calculate its characteristic age $\tau_c = 2870$ yr and current spin-down luminosity $L(t_{age}) = 1.18 \times 10^{37}$ erg s^{-1}. In our work, we assumed that the distance equals 6 kpc, same distance is also adopted by Zhu et al. (2018). In addition, for the ejected mass and supernova remnant explosion energy, we adopted same values with Crab Nebula, $M_{ej} = 9.5M_\odot$ and $E_0 = 1 \times 10^{51}$ erg. For the PWN G54.1+0.3, its age is uncertain and different studies suggested it lies in different ranges (e.g., Camilo et al. (2002): 1500-6000 yr, Bocchino et al. (2010): 1800–2400 yr, Gelfand et al. (2015): 2100–3600 yr) or different certain values (e.g., Torres et al. (2014): 1700 yr, Zhu et al. (2018): 2600 yr) and we assumed $\tau_{age} = 2600$ yr. The initial luminosity $L_0 = 1.34 \times 10^{39}$ erg s^{-1} and initial spin-down timescale $\tau_0 = 269$ yr.

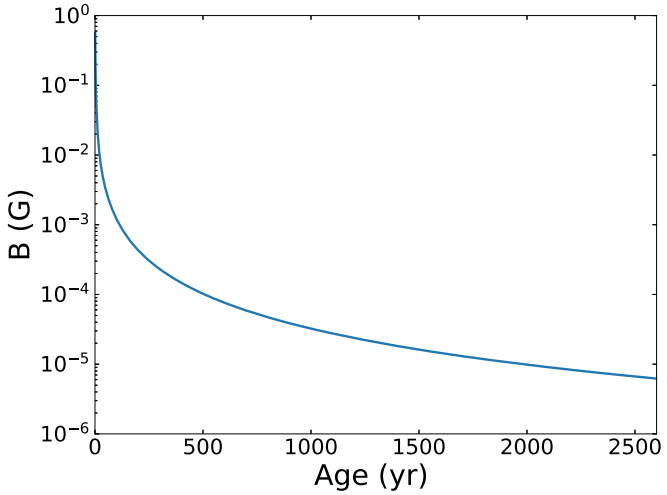

Figure 1. Magnetic field as a function of time for PWN G54.1+0.3 with $\eta = 0.004$.

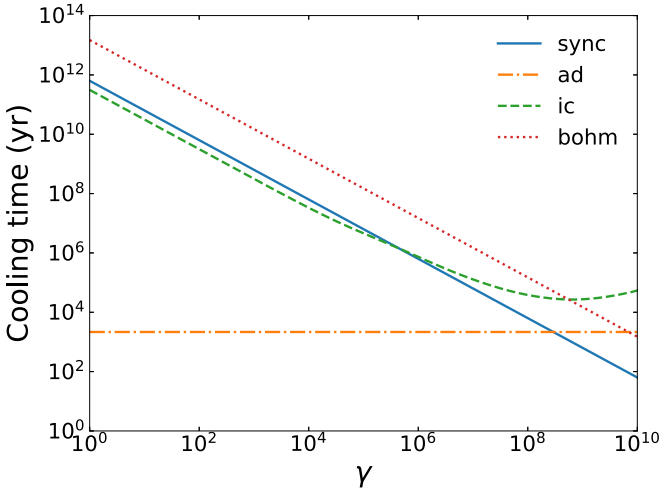

Figure 2. Cooling times for the different losses (synchrotron radiation, adiabatic losses, inverse Compton scatting and Bohm diffusion) at $t_{\rm age} =$ 2600 yr.

With $t_{\rm age} = 2600$ yr, we assumed $\eta = 0.004$ and calculated the magnetic field strength in the nebula using Equation (3). The evolution of magnetic field over time is explained in Figure 1. As shown in the figure, due to the expansion of the PWN resulting in the weakening of the synchrotron radiation, the magnetic field strength decreases at a fast and then slow speed over time and it equals 6.22 μG at $t_{\rm age} = 2600$ yr. The timescales of the particles for the cooling of the synchrotron radiation, the adiabatic loss, the inverse Compton scattering, and the escape are illustrated in Figure 2. For $\gamma < 6 \times 10^8$, the adiabatic loss is the dominant process to cool the particles, Whereas the synchrotron radiation becomes the most prominent mechanism for $6 \times 10^8 < \gamma < 1 \times 10^{10}$. In order to calculate the spectral energy distribution (SED) for the inverse Compton scattering of the high-energy particles off the background soft photons, the energy densities of the fields is obtained based on the radiation transfer model for the Milky Way (Popescu et al. 2017), which are listed in Table 2. The radio fluxes for the G54.1+0.3 are collected from different studies and listed in Table 1. The PWN is also observed in the X-ray band with the ROSAT PSPC, Lu et al. (2001) give the flux of G54.1+0.3 at 1 keV, $F_{\rm 1keV} = 6.4 \times 10^{-4}$ mJy.

The GeV γ-ray band data is obtained by analyzing about 14 yr of Fermi-LAT data (Fermi Mission Elapsed Time 239557417s-676515024s). After filtering the data with the commands *gtselect*, *gtmktime*, we used the isotropic γ-ray background emission (`iso_P8R3_SOURCE_V3_v1`) and the diffuse Galactic interstellar emission (`gll_iem_v07`) to model the background. Then we adopted the model of 4FGL J1930.5+1853 (logged in 4FGL-DR3 as the GeV counterpart of G54.1+0.3; Abdollahi et al. 2022) to create the SED between the 800 MeV to 200 GeV band. For TeV energies, the fluxes are obtained from Albert et al. (2020, 2023), and Cao et al. (2023).

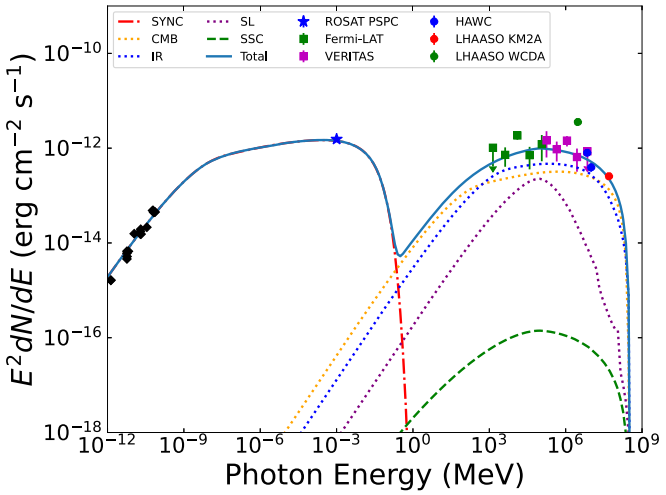

Figure 3. The SED from a broken power law model for PWN G54.1+0.3. The dependent parameters are shown in Table 2. The observed fluxes in radio, X-rays with ROSAT PSPC (Lu et al. 2001), γ-rays with Fermi LAT (this work), VERITAS (Abeysekara et al. 2018), HAWC (Albert et al. 2020, 2023), and LHAASO (Cao et al. 2023) are also indicated.

At $t_{\rm age} = 2600$ yr, $\eta = 0.004$ and $\epsilon = 0.3$, we assumed the particles are injected into the nebula with a broken power law (model A) and obtained the SED of PWN G54.1+0.3 with a set of reasonable parameters: $\alpha_1 = 1.4$, $\alpha_2 = 2.7$, $\gamma_{\rm b} = 5 \times 10^5$ and $\eta = 0.004$. All of parameters are summarized in Table 2. As shown in Figure 3, the resulting SED is consistent with the detected γ-ray fluxes with Fermi-LAT, VERITAS, HAWC, and LHAASO, which indicates that PWN G54.1+0.3 is capable of generating the UHE γ-ray radiation of 1LHAASO J1929 +1846. The synchrotron radiation contributes prominently the non-thermal emission from the radio to the X-ray band. There

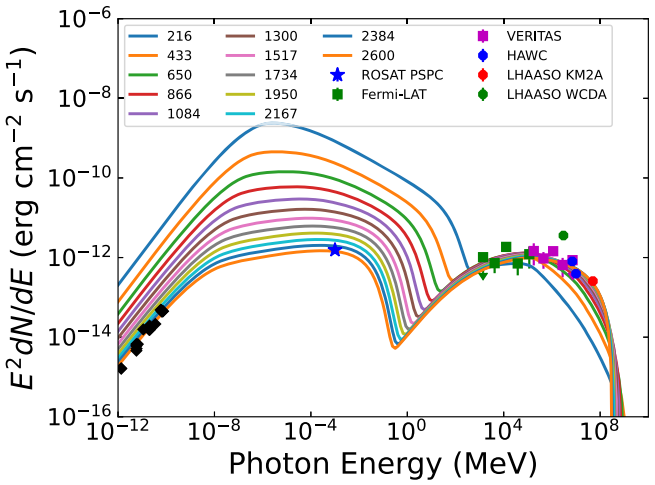

Figure 4. The SEDs at different times from a broken power law model for PWN G54.1+0.3. The observed fluxes are the same as Figure 3.

Table 1
Integrated Flux Densities from the Literature for PWN G54.1+0.3

ν/GHz	S_i/mJy	Reference
0.327	495 ± 75	Velusamy & Becker (1988)
0.327	504 ± 17	Taylor et al. (1996)
1.4	478 ± 30	Velusamy & Becker (1988)
1.4	327.5 ± 10.9	Condon et al. (1989)
1.42	364 ± 36	Caswell & Haynes (1987)
1.6	417 ± 30	Velusamy & Becker (1988)
2.7	580 ± 60	Reich et al. (1984)
4.75	370 ± 40	Reich et al. (1985)
4.8	325 ± 20	Velusamy & Becker (1988)
4.875	400 ± 40	Altenhoff et al. (1979)
5.0	306 ± 31	Griffith et al. (1990)
1.4	433.0 ± 30	Lang et al. (2010)
4.7	327.0 ± 25	Lang et al. (2010)
8.5	252.0 ± 20	Lang et al. (2010)

are a spectrum break between the radio and the X-ray band at $\sim 1 \times 10^{-8}$ MeV and a cutoff at $\sim 10^{-2}$ MeV. The changing of spectrum index causing the break and the value of γ_b decides the break. In the γ-ray band, the inverse Compton scattering off with the infrared (IR) and the cosmic-microwave background (CMB) soft photons is the most prominent contributor to the high-energy emission, and the self-synchrotron Compton (SSC) process is negligible in producing the γ-rays with the magnetic field strength of 6.22 μG.

With parameters of the model A, we studied the SEDs of PWN G54.1+0.3 at different times resulting in Figure 4. During the evolution of nebula, nebula keeps expanding and its radius enlarges, and then magnetic fields decrease, thus synchrotron radiation diminishes markedly over time. And the break energy and cutoff energy also decrease about two orders of magnitude. The peak fluxes produced via synchrotron

Table 2
Parameters for PWN G54.1+0.3

Parameters	Symbol	Value
Pulsar and eject parameters		
Period (ms)	$P(t_{age})$	136
Period derivative (s s^{-1})	$\dot{P}(t_{age})$	7.5×10^{-13}
Breaking index	n	3
Characteristic age (yr)	τ_c	2870
Initial spin-down age (yr)	τ_0	269
Spin-down luminosity now (erg s^{-1})	$L(t_{age})$	1.18×10^{37}
Initial spin-down luminosity (erg s^{-1})	L_0	1.34×10^{39}
Ejected mass ($M_\odot$)	M_{ej}	9.5
SN explosion energy (erg)	E_0	1×10^{51}
Distance (kpc)	d	6.0
Environment parameters		
CMB temperature (K)	T_{CMB}	2.73
CMB energy density (eV cm^{-3})	U_{CMB}	0.25
IR temperature (K)	T_{IR}	32
IR energy density (eV cm^{-3})	U_{IR}	0.55
Star light temperature (K)	T_{SL}	3000
Star light energy density (eV cm^{-3})	U_{SL}	1.15
Particles and field parameters		
Breaking energy	γ_b	5×10^5
Low energy index	α_1	1.4
High energy index	α_2	2.7
Magnetic fraction	η	0.004
Shock radius fraction	ϵ	0.3

radiation and inverse Compton scattering also decreased. Furthermore, in TeV energies, the decreasing trend of γ-ray emission is not obvious as radio and X-ray emission. However, from $\sim$1 MeV to $\sim 1 \times 10^4$ MeV, the fluxes produced via inverse Compton scattering and the shape of spectrum keep same almost at different age stages.

The previous studies with a similar model with a broken power law limited separately spectral indexes in the range of 1.0–1.6 and 2.2–2.8 (Torres et al. 2014) or 1.00–.75 and 2.09–3.08 (Zhu et al. 2018) for α_1 and α_2. On the basis, we tried to finding another prefer spectral indexes keeping other parameters invariable with model A. Resulting SEDs with different α_1 and α_2 are illustrated in Figure 5. Solid green line with model A ($\alpha_1 = 1.4$, $\alpha_2 = 2.7$), dashed blue line with $\alpha_1 = 1.0$, $\alpha_2 = 2.8$, and dashed orange line with $\alpha_1 = 1.7$, $\alpha_2 = 2.6$ show three different SEDs of PWN G54.1+0.3. Obviously, the reproduced fluxes at the X-ray band for the dashed blue line ($\alpha_1 = 1.0$, $\alpha_2 = 2.8$) and the GeV energies for the dashed orange line ($\alpha_1 = 1.7$, $\alpha_2 = 2.6$) are lower than the fluxes detected with the ROSAT PSPC and the Fermi-LAT. Only the solid green line can fit well with most of the fluxes detected by the different detectors, including radio, X-ray, and γ-ray energies. Overall, the spectral indexes ($\alpha_1 = 1.4$, $\alpha_2 = 2.7$) of Model A are the relatively most reasonable ones.

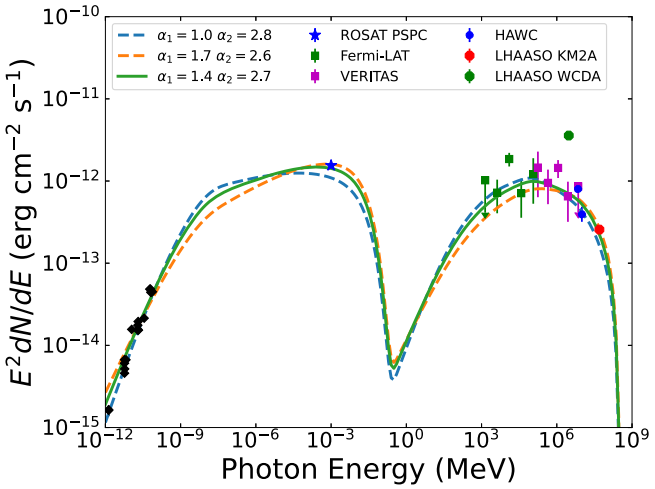

Figure 5. The SEDs from a broken power law model for PWN G54.1+0.3 with different spectral indexes, α_1 and α_2: the solid green line with model A ($\alpha_1 = 1.4$, $\alpha_2 = 2.7$), the dashed blue line with $\alpha_1 = 1.0$, $\alpha_2 = 2.8$, and the dashed orange line with $\alpha_1 = 1.7$, $\alpha_2 = 2.6$. The dependent parameters and the observed fluxes are the same as Figure 3.

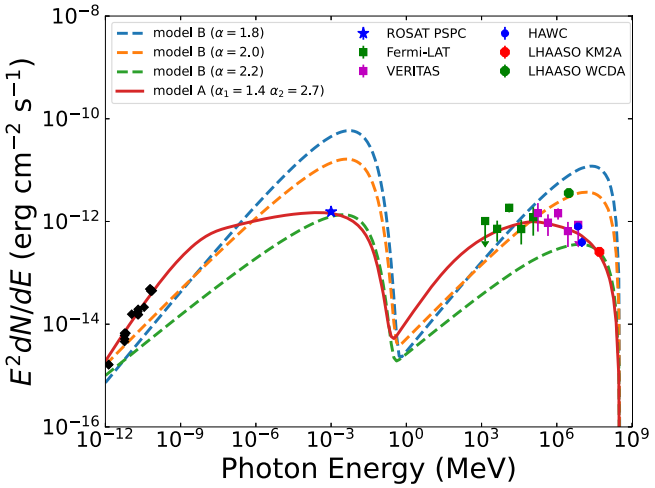

Figure 6. Comparison of SEDs with a spectrum of a power law (model B) with different spectral indexes: the dashed blue line with $\alpha = 1.8$, the dashed orange line with $\alpha = 2.0$, the dashed green line with $\alpha = 2.2$, and a broken power law (model A, $\alpha_1 = 1.4$, $\alpha_2 = 2.7$) for the injected particles. The dependent parameters and the observed fluxes are the same as Figure 3.

We also examined the scenario where particles are injected with a power law, while keeping all parameters constant except for the spectral index. Figure 6 illustrates that when we vary the spectral index for this model (model B), it cannot well reproduce the fluxes in radio and γ-rays. For the dashed blue line for $\alpha = 1.8$ and the dashed orange line for $\alpha = 2.0$, it is evident that the resulting fluxes are lower than the observed fluxes at the radio and the GeV bands, but higher at the X-ray and TeV bands. The dashed green line with $\alpha = 2.2$ can only reproduce the observed fluxes in the X-ray band, as well as the lower fluxes detected by HAWC and the flux detected by LHAASO KM2A. Regardless of how we adjust the spectral index, the broken power law model remains the better scenario for reproducing the observed γ-ray fluxes than the power law one.

The observation positions of VER J1930+188 and HAWC J1930+188 agree well with G54.1+0.3, and the PWN is the most likely counterpart of the TeV emission (Albert et al. 2020, 2023). The γ-ray emitter associated with VER J1930+188 and HAWC J1930+188 is the only source with energy above 50 GeV within the region of $0^\circ.3$ from 1LHAASO J1929+1846 (Cao et al. 2023). It is reasonable to argue that the UHE radiation of 1LHAASO J1929+1846 originates from PWN G54.1+0.3, despite a spatial offset of $0^\circ.29$ between them. Furthermore, as shown in Figure 3, the flux at 3 TeV detected by WCDA is higher than those detected by VERITAS, and HAWC, which is probably because a rather large extension with a radius of $r_{39} = 0^\circ.49$ is adopted in deriving the flux from the data with WCDA. We expect that future observations from LHAASO will further aid in the study of the UHE γ-ray emission properties of 1LHAASO J1929+1846.

4. Summary and Discussion

We investigated the multiband non-thermal emission of PWN G54.1+0.3 based on a one-zone time-dependent model for the multiband non-thermal emission for PWNe with reasonable parameters to explore whether the nebula is able to possess energetic particles to produce the UHE γ-rays of 1LHAASO J1929+1846. The observed fluxes used in our paper are provided with different detectors, ROSAT PSPC, Fermi-LAT, VERITAS, HAWC and LHAASO, and those in radio band. We assumed the particles (electrons and positrons) are injected sequentially into the PWN with the broken power law (model A) and the power law (model B), respectively.

For model A with $\alpha_1 = 1.4$, $\alpha_2 = 2.7$, $\gamma_b = 5 \times 10^5$, $\epsilon = 0.3$ and $\eta = 0.004$, the resulting SED for PWN G54.1+0.3 agrees well with the detected results from the radio to the TeV band. The result indicates that PWN G54.1+0.3 is capable of producing the γ-ray flux of 1LHAASO J1929+1846 with reasonable parameters. We also investigated a scenario where particles are injected with a power law distribution, while keeping all other parameters constant except for the spectral index. However, no matter how we adjust the spectral index, the broken power law model consistently provides a better fit to the observed gamma-ray fluxes. Thus, we can conclude that the broken power law model is more appropriate for reproducing the observed fluxes than the power law model.

At $t_{\rm age} = 2600$ yr, we assumed $\eta = 0.004$ and calculated the magnetic field strength $B = 6.22$ μG, which is smaller than

$B = 9.48$ μG in Zhu et al. (2018) with $\eta = 0.0045$. The smaller value of η results in this difference. The spin-down energy of the pulsar is injected into the particles and the magnetic field in the PWN and the high-energy particles accumulate over time. We assumed an older age of G54.1+0.3, 2600 yr, which leads to a higher initial luminosity $L_0 = 1.34 \times 10^{39}$ erg s^{-1} compared with $L_0 = 7.2 \times 10^{37}$ erg s^{-1} derived by Torres et al. (2014) with $t_{\rm age} = 1700$ yr.

Acknowledgments

This work is supported by the National Natural Science Foundation of China (NSFC) through grants U2031107 and 12063004, the grant from Yunnan Province (YNWR-QNBJ-2018-049), Yunnan Fundamental Research Projects (grant No. 202201BF070001-020), and the 14th Graduate Research and Innovation Project of Yunnan University (grant No. KC-22221016).

References

Abdollahi, S., Acero, F., Baldini, L., et al. 2022, ApJS, 260, 53
Abeysekara, A. U., Albert, A., Alfaro, R., et al. 2020, PhRvL, 124, 021102
Abeysekara, A. U., Archer, A., Benbow, W., et al. 2018, ApJ, 866, 24
Albert, A., Alfaro, R., Alvarez, C., et al. 2020, ApJ, 905, 76
Albert, A., Alfaro, R., Alvarez, C., et al. 2023, ApJ, 942, 96
Altenhoff, W. J., Downes, D., Pauls, T., & Schraml, J. 1979, A&AS, 35, 23
Bocchino, F., Bandiera, R., & Gelfand, J. 2010, A&A, 520, A71
Camilo, F., Lorimer, D. R., Bhat, N. D. R., et al. 2002, ApJL, 574, L71
Cao, Z. 2010, CPC, 34, 249
Cao, Z., Aharonian, F., An, Q., et al. 2023, arXiv:2305.17030
Cao, Z., Aharonian, F. A., An, Q., et al. 2021, Natur, 594, 33
Caswell, J. L., & Haynes, R. F. 1987, A&A, 171, 261
Condon, J. J., Broderick, J. J., & Seielstad, G. A. 1989, AJ, 97, 1064
Fang, J., Wen, L., Yu, H., & Chen, S. 2020, MNRAS, 498, 4901
Gelfand, J. D., Slane, P. O., & Temim, T. 2015, ApJ, 807, 30
Griffith, M., Langston, G., Heflin, M., et al. 1990, ApJS, 74, 129
H. E. S. S. Collaboration, Abdalla, H., Abramowski, A., et al. 2018, A&A, 612, A1
Joshi, J. C., Tanaka, S. J., Miranda, L. S., & Razzaque, S. 2023, MNRAS, 520, 5858
Lang, C. C., Wang, Q. D., Lu, F., & Clubb, K. I. 2010, ApJ, 709, 1125
Liang, X.-H., Li, C.-M., Wu, Q.-Z., Pan, J.-S., & Liu, R.-Y. 2022, Univ, 8, 547
Liu, R.-Y., & Wang, X.-Y. 2021, ApJ, 922, 221
Lu, F., Wang, Q. D., Gotthelf, E. V., & Qu, J. 2007, ApJ, 663, 315
Lu, F. J., Aschenbach, B., & Song, L. M. 2001, A&A, 370, 570
Lu, F. J., Wang, Q. D., Aschenbach, B., Durouchoux, P., & Song, L. M. 2002, ApJL, 568, L49
Martín, J., Torres, D. F., & Rea, N. 2012, MNRAS, 427, 415
Popescu, C. C., Yang, R., Tuffs, R. J., et al. 2017, MNRAS, 470, 2539
Reich, W., Fuerst, E., Altenhoff, W. J., Reich, P., & Junkes, N. 1985, A&A, 151, L10
Reich, W., Fuerst, E., Haslam, C. G. T., Steffen, P., & Reif, K. 1984, A&AS, 58, 197
Tanaka, S. J., & Takahara, F. 2010, ApJ, 715, 1248
Taylor, A. R., Goss, W. M., Coleman, P. H., van Leeuwen, J., & Wallace, B. J. 1996, ApJS, 107, 239
Torres, D. F., Cillis, A., Martín, J., & de Oña Wilhelmi, E. 2014, JHEAp, 1, 31
van der Swaluw, E., Achterberg, A., Gallant, Y. A., & Tóth, G. 2001, A&A, 380, 309
Velusamy, T., & Becker, R. H. 1988, AJ, 95, 1162
Wu, K., Zhou, L., Gong, Y., & Fang, J. 2023, MNRAS, 519, 1881
Yu, H., Wu, K., Wen, L., & Fang, J. 2022, NewAs, 90, 101669
Zhang, X., Chen, Y., Huang, J., & Chen, D. 2020, MNRAS, 497, 3477
Zhu, B.-T., Zhang, L., & Fang, J. 2018, A&A, 609, A110